Methods of acoustic gas flux inversion—Investigation into the initial amplitude of bubble excitation

Ben Roche ; Paul R. White ; Jonathan M. Bull; Timothy G. Leighton ; Jianghui Li; Colin Christie; Joseph Fone

Check for updates

View Online Export Citation

The Journal of the Acoustical Society of America

Methods of acoustic gas flux inversion—Investigation into the initial amplitude of bubble excitation

Ben Roche,[1,a] Paul R. White,[2] Jonathan M. Bull,[1] Timothy G. Leighton,[2] Jianghui Li,[1] Colin Christie,[1] and Joseph Fone[1]

[1]*School of Ocean and Earth Science, National Oceanography Centre Southampton, University of Southampton Waterfront Campus, European Way, Southampton, United Kingdom*

[2]*Institute of Sound and Vibration Research, University of Southampton, Southampton, United Kingdom*

ABSTRACT:

Passive acoustic inversion techniques for measuring gas flux into the water column have the potential to be a powerful tool for the long-term monitoring and quantification of natural marine seeps and anthropogenic emissions. Prior inversion techniques have had limited precision due to lack of constraints on the initial amplitude of a bubble's excitation following its release into the water column ($R_{\varepsilon 0i}$). $R_{\varepsilon 0i}$ is determined by observing the acoustic signal of bubbles released from sediment in a controlled experiment and its use is demonstrated by quantifying the flux from a volcanic CO_2 seep offshore Panarea (Italy), improving the precision by 78%.

© *2022 Author(s). All article content, except where otherwise noted, is licensed under a Creative Commons Attribution (CC BY) license (http://creativecommons.org/licenses/by/4.0/).* https://doi.org/10.1121/10.0013220

I. INTRODUCTION

In recent years, there has been a growing need to refine methods for quantifying the volume of gas released into the water column from marine sediments. This demand is fueled by a need to better understand the natural carbon cycle and a requirement to measure, monitor, and verify offshore carbon capture and storage (CCS) sites.[1–6] While there are a variety of techniques to quantify gas emissions, including direct physical measurements, many of these are severely limited in terms of applicability in regard to spatial and temporal coverage, as well as cost. Optical techniques are generally accurate for a limited bubble size range (bubbles large enough to be accurately resolved) but limited in the area they can survey and dependent on water visibility.[7–9] Active acoustic techniques, although able to cover a large area, require time-consuming processing to provide accurate quantification data and give only a snapshot measurement.[10–15] Furthermore, the accuracy of the assumptions that underpin the conversion of active acoustic data into gas fluxes is still evolving.[10] Passive acoustic inversion techniques, on the other hand, are low energy and capable of long-term deployments in any level of visibility and also provide information about the size distribution of bubbles released from the seep.[7,16–21]

Passive acoustic inversion relies on a physical model of the sound emitted by a bubble as it is formed. Originally, this principle was restricted to measuring the size of individual bubbles in low flux environments, via the so-called signature method, to ensure the acoustic signature of bubbles did not overlap.[22–25] This approach relies on knowing the frequency emitted by a bubble immediately after release, which is directly related to its equilibrium radius.[19,24,26,27]

Signal processing methods were developed to allow this technique to extend to intermediate flux rates when bubble signatures begin to overlap.[28] For high flux rates, when bubble signatures do overlap to a significant degree, an approach based on the spectral density of the acoustic pressure measured in the far field at a known distance from a gas seep is appropriate.[21,29] Using a model of the spectrum of the signature of each bubble formation event, the measured spectrum can be used to infer the bubble size distribution. However, the energy released by an individual bubble remains poorly characterized,[21] particularly, how it varies with depth and mode of injection. This quantity directly affects the gas flux estimate, for example, if the model assumes the bubble is a stronger sound source than it is, then the inversion will underestimate the gas flux.[21] Conversely, if a single bubble emits more energy than predicted by the model, then the passive acoustic inversion will overestimate the gas flux. To date, the use of the spectral method in the field has proven effective, providing continuous estimates of gas flux over extended periods of time validated by intermittent physical and optical measurements. Unfortunately, such estimates have contained large uncertainties.[7,19,30]

This study examines the acoustic signature of bubbles released from coarse-grained sediment to improve the spectral inversion approach by examining the energy released by an individual bubble and the relationship between the initial radius of excitation of a bubble and the equilibrium radius of a bubble. It should be noted at this stage, while a bubble released into the water column may not be spherical, the use of a radial displacement as a descriptor is common in

a)Electronic mail: br4g13@soton.ac.uk

literature as a proxy for more complex volumetric descriptions as (a) the zeroth-order spherical harmonic displacement was the only one that changed bubble volume (to first order) and so radiated a spherical pressure wave,[27] and (b) because this aligned the formulation with the historical use in the West of representing bubble volume by an equivalent spherical bubble of known radius.[31] We then use this refined acoustic inversion technique to quantify ebullition from a natural CO_2 seep occurring at a site with coarse-grained sediment and compare the estimate to physical and simultaneous optical measurements.

A. The spectral method—Model of acoustic emissions from a bubble

The following summarizes the mathematical model for the sound from a plume, which forms the basis of the inversion approach. The theory assumes that the acoustic pressure signature from a single bubble is an exponentially decaying sinusoid.[21]

For a spherical bubble, immediately after being entrained into the water column, a bubble will undergo damped simple harmonic motion. The radius of a bubble, R, over time, t, can be described by

$$R(t) = \text{Re}\left(R_0 - R_{\varepsilon 0i} e^{j\omega_0(t-t_\vartheta)} e^{-\omega_0 \delta_{\text{tot}}(t-t_\vartheta-t_i)/2} H(t-(t_\vartheta-t_i)) \right),$$
(1)

where Re denotes the real part of a complex number, δ_{tot} is the total damping coefficient, H is the Heaviside step function, t_i is the moment when the acoustic signal is first detected, t_ϑ accounts for the propagation time between perturbations of the bubble and the corresponding pressure signal at the receiver, $t_i - t_\vartheta$ is the moment when the bubble begins to oscillate, R_0 is the equilibrium radius of the bubble, and $R_{\varepsilon 0i}$ is the initial amplitude of displacement of the bubble wall.[21]

The natural angular frequency, ω_0, of the bubble is given by an extended form of Minnaert's equation,[19,27]

$$\omega_0 = \frac{1}{R_0 \sqrt{\rho_0}} \sqrt{3\kappa\left(p_0 - p_v + \frac{2\sigma}{R_0}\right) - \frac{2\sigma}{R_0} + p_v - \frac{4\eta^2}{\rho_0 R_0^2}},$$
(2)

where κ is the polytropic index of the gas in the bubble, p_0 is the ambient pressure outside of the bubble, p_v is the gas' vapour pressure, ρ_0 is the density of surrounding liquid, and η is the liquid's shear viscosity.

The oscillating bubble wall creates an acoustic pressure in the far field at a distance, r, given by

$$P(t) \approx \text{Re}\left\{ \rho_0 \frac{(\omega_0 R_0)^2}{r} R_{\varepsilon 0i} e^{j\omega_0(t-t_\vartheta)} e^{-\omega_0 \delta_{\text{tot}}(t-t_\vartheta-t_i)/2} H(t-t_i) \right\}.$$
(3)

The squared magnitude of the Fourier transform of the pressure radiated from a single bubble at a distance, r, is

$$|X(\omega, R_0)|^2$$
$$= \left[\omega_0^2 R_0^3 \frac{\rho_0}{r} \frac{R_{\varepsilon 0i}}{R_0} \right]^2$$
$$\times \left(\frac{4\left[(\omega_0 \delta_{\text{tot}})^2 + 4\omega^2\right]}{\left[(\omega_0 \delta_{\text{tot}})^2 + 4(\omega_0 - \omega)^2\right]\left[(\omega_0 \delta_{\text{tot}})^2 + 4(\omega_0 + \omega)^2\right]} \right).$$
(4)

The spectrum, $S(\omega)$, of the measured acoustic pressure from a population of bubbles with size distribution $D(R_0)$, which is defined such that $\int_{R_1}^{R_2} D(R_0) dR_0$ represents the number of bubbles generated per second with a radius in the range (R_1, R_2) can be expressed as

$$S(\omega) \approx \int_0^\infty D(R_0) |X(\omega, R_0)|^2 dR_0.$$
(5)

To estimate the number of bubbles via the far field acoustic signal, one needs to determine what value of $D(R_0)$ generates the measured power spectrum, $S(\omega)$. This can be achieved by discretising Eq. (5) into N_b finite radii bins such that the nth radius bin is centered on the radius, R_n^c. Assuming that the bins are contiguous, the power spectrum can be given as

$$S(\omega) \approx \sum_{n=1}^{N_b} \Psi(n) |X(\omega, R_n^c)|^2,$$
(6)

where $\Psi(n)$ is the bubble generation rate within a radius bin (i.e., the number of bubbles formed per second within the nth radius bin) such that $\Psi(n) = (R_{n+1}^c - R_n^c) D(R_n^c)$. The spectrum can be evaluated at the N_f discrete frequencies, ω_m, and organized into a column vector, $\underline{S}$, allowing Eq. (6) to be written in matrix form,

$$\underline{S} = M\underline{\Psi},$$
(7)

where $\underline{\Psi}$ is a column vector containing the elements $\Psi(n)$, and M is an $(N_f \times N_b)$ matrix with elements $\{M\}_{m,n} = |X(\omega_m, R_n^c)|^2$.

The matrix equation (7) can be solved for the number of bubbles generated per second $\underline{\Psi}$ in a radius bin, provided that $\underline{S}$ and M are known, to yield an estimate of the gas flux. However, while $\underline{S}$ can easily be determined accurately with the use of a calibrated hydrophone, M remains difficult to accurately determine. This is because Eq. (4) contains one important unknown value, the initial amplitude of the displacement of the bubble wall when it begins to oscillate, $R_{\varepsilon 0i}$. Most work on studying this has assumed a model of the form, $R_{\varepsilon 0i} = \chi_{\text{rad}} R_0$, where χ_{rad} is a constant, representing the ratio of the initial amplitude of displacement of the bubble radius and equilibrium radius. The earliest estimate of χ_{rad} for bubbles of radii close to 0.001 mm measured near a small waterfall suggested that[24] $\chi_{\text{rad}} = 10^{-5}$, and the same data were reanalyzed using a more sophisticated model to yield[32] $\chi_{\text{rad}} = 10^{-4}$. And, considering data from smaller

800   J. Acoust. Soc. Am. **152** (2), August 2022

Roche *et al.*

bubbles ($R_0 \approx 0.000\,312$ m) generated in breaking waves suggested[33] that $\chi_{\text{rad}} = 1.5 \times 10^{-2}$. Generating bubbles via sheared flows allowed the number of bubbles (>1000) and the range of radii ($R_0 = 0.0001$–0.001 m) measured to be greatly expanded.[34] This work suggested that χ_{rad} was not a constant and increased with decreasing bubble size. Further, in this data, χ_{rad} was seen to vary by up to 2 orders of magnitude. One approach to estimating χ_{rad} is to compute the flux of bubbles in an experiment where the flux rate can be controlled and measured directly; such an approach has been found to yield estimates of χ_{rad} between[19] 1.4×10^{-4} and 5.6×10^{-4}. The apparent variable nature of χ_{rad} across bubble sizes and release mechanisms potentially introduces considerable uncertainty into derived flux estimates.[19]

None of these estimates for the initial amplitude are based on bubbles emerging from sediments. Further, these estimated values are based on a small set of environmental conditions, for example, they are the range of bubble sizes and generation mechanisms.[19] Consequently, there is a need for calibrated $R_{\varepsilon 0 i}$ values, particularly in conditions replicating those found in the field. This paper undertakes such an exercise.

The experimental evidence supporting the assumption that χ_{rad} is a constant is rather weak. Herein, the general approach based on assuming $R_{\varepsilon 0 i}$ is a function of R_0, i.e., $R_{\varepsilon 0 i} = f(R_0)$, is adopted so that Eq. (4) becomes

$$
\begin{aligned}
&\left| X(\omega, R_0) \right|^2 \\
&= \left[\frac{f(R_0)\omega_0{}^2 R_0{}^2 \rho_0}{r} \right]^2 \\
&\quad \times \left(\frac{4\left[(\omega_0 \delta_{\text{tot}})^2 + 4\omega^2 \right]}{\left[(\omega_0 \delta_{\text{tot}})^2 + 4(\omega_0 - \omega)^2 \right]\left[(\omega_0 \delta_{\text{tot}})^2 + 4(\omega_0 + \omega)^2 \right]} \right).
\end{aligned}
$$

(8)

In this study, we analyze the acoustic emissions from 368 bubbles released from sediment into the water column to determine the $R_{\varepsilon 0 i}$, measuring the frequency of each bubble oscillation alongside the maximum radius of excitation and total energy released.

II. METHODOLOGY

A. Experimental design

To measure and analyze the acoustic signature of bubbles released from sediment, air was injected into the base of ~ 0.30 m of artificial sediment with resulting emissions into the water column recorded with a calibrated hydrophone [Reson TC 4032, Teledyne Technology, Alton, with a sensitivity of 167 dB re 1 V/μPa at 1 m; 0.30 m above the sediment surface; Figs. 1(a) and 1(b)]. Synthetic sediment (Ballotini; 0.009 m diameter, pebbly gravel on the Wentworth scale) was used to ensure uniformity between the grains and simplify porosity and permeability calculations [Fig. 1(c)]. The experiment was designed so that ebullition was in the center of a large 8 m $\times$ 8 m ($\times$ 5 m deep) freshwater tank [Fig. 1(a)] to reduce the interference of wall
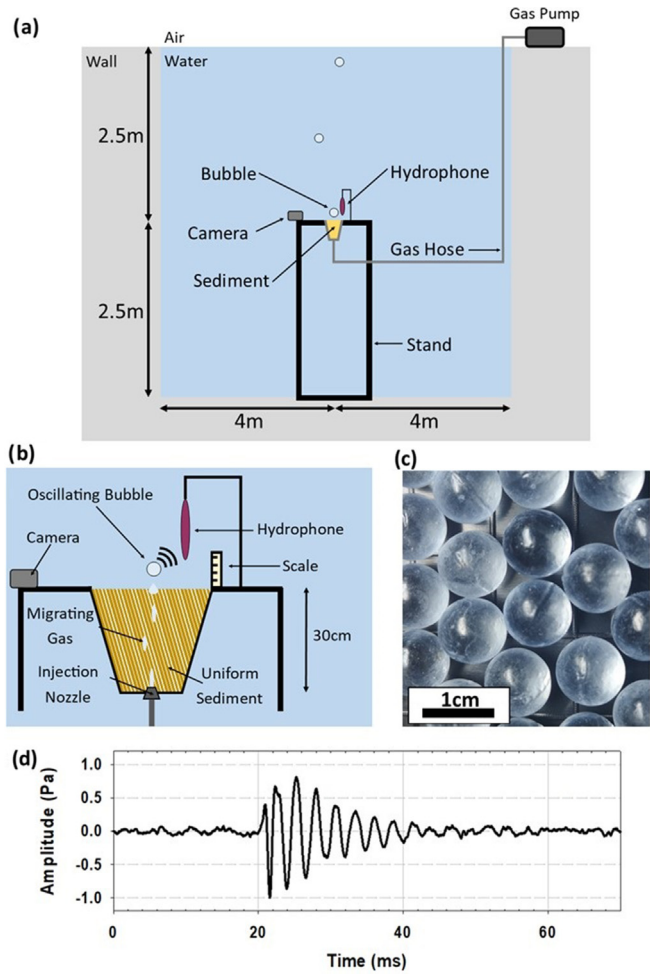

FIG. 1. (Color online) Experimental design. (a) A schematic showing gas injection at base of sediments and the position of optical and acoustic sensors within the water tank; (b) detailed schematic; (c) image of the Ballotini sediment used for the experiment; and (d) sonogram displaying the typical acoustic emission of a bubble as recorded by the hydrophone.

reflections, allowing accurate characterization of the acoustic signatures [Fig. 1(d)]. The gas injection rate at the base of the sediment was adjusted until gas migration through the sediment caused bubbles to enter the water column at less than 1 bubble per second. Bubble radii were determined directly from optical measurements (Sony FDR3000 camera, Minato, Japan; 0.50 m from ebullition site).

The optical footage was used to identify periods where single, discrete bubbles entered the water column to ensure that the acoustic signature of an individual bubble release was analyzed. The acoustic and optical data for each bubble were jointly analyzed to determine the start and end time of the bubble oscillation, as well as the maximum pressure of the bubble signal ($P_{\max}$). The initial excitation radius of the bubble ($R_{\varepsilon 0 i}$) is then calculated using the pressure signals via [21,34]

$$
R_{\varepsilon 0 i} = \frac{r}{3\kappa p_0} P_{\max},
$$

(9)

where $P_{\max}$ is the maximum pressure signal recorded at the hydrophone as a result of the bubble oscillation.

Roche *et al.*   801

The center frequency of each bubble signature was determined by iteratively fitting an exponential decaying sinusoid to the signal based on least squares error criterion. The frequency of this wave was used to calculate the equilibrium bubble radius, R_0, using Eq. (2). The total energy of each bubble oscillation was determined by integrating the acoustic pressure squared as recorded at the hydrophone between the start (t_1) and end (t_2) of the event. This is corrected for range, assuming spherical spreading.

$$E = \frac{1}{fs} \frac{4\pi r^2}{2\rho_0 c} \sum_{t_1}^{t_2} |P(t)^2|, \qquad (10)$$

where c is the speed of sound in water ($1500\,\text{ms}^{-1}$) and fs is the sampling frequency (96 kHz). To account for background noise (electrical and acoustic), the ambient noise on the measurement was calculated using Eq. (10) with the average energy measured over 1 s being equal to 6.2×10^{-9} J. Subsequently, $6.2 \times 10^{-9}(t_2 - t_1)$ J were subtracted from each event so that only the energy of the bubble oscillation was observed.

B. Validation using field data

To validate these observations, acoustic data collected from a natural seep in offshore Panarea (Bottaro Crater),

Italy, is inverted and the estimated flux compared to that obtained by physical bottle measurements collected by a diver and estimates made from simultaneous optical measurements. Panarea is a small Aeolian Island in the southern Tyrrhenian Sea, ~20 km SW of the active volcano Stromboli (Fig. 2). As a result of the underlying magma chamber, the waters surrounding the island are host to numerous natural CO_2 seeps.[35–38] The calm clear shallow waters surrounding Panarea make it an ideal natural laboratory for testing ebullition detection and quantification techniques.[39–41] Bubbles from the target seep were released from coarse-grained sediment at a rate of approximately 5 bubbles per second, directly comparable to our tank experiment. Similarly, bubbles released from the seep ranged in size from 0.001 to 0.008 m comparable to the 0.003–0.012 m observed in the tank [Fig. 2(c)]. The seep was, however, located at a depth of 12 m, compared to the depth of 2.5 m in the experiments.

Analysis focusses on 10 min of simultaneous optical and acoustic data acquired using an open frame lander, incorporating a calibrated hydrophone (Geospectrum M36, GTI, Dartmouth, Nova Scotia, Canada), and two inward facing Sony FDR-X3000 cameras, focussing on a single central point with scale boards positioned directly opposite. Optical data were processed using techniques described in Li *et al.*, where the radius of each bubble was calculated from the
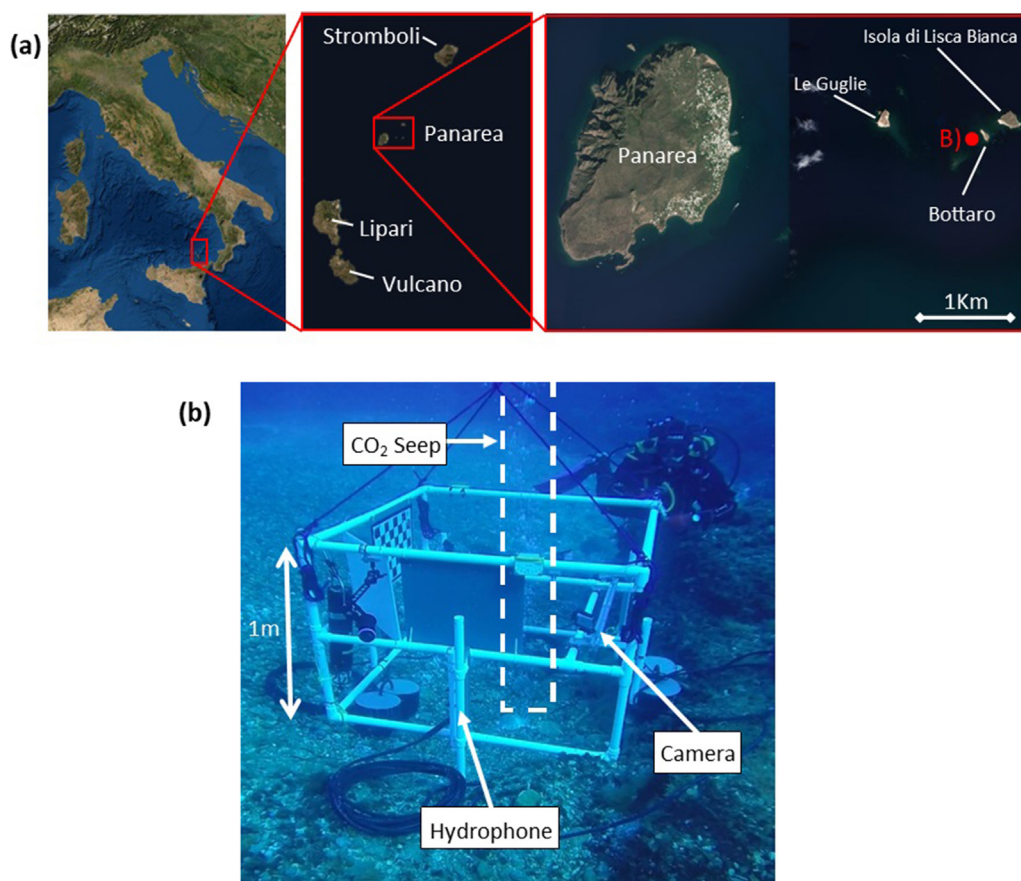

FIG. 2. (Color online) The field work location map showing (a) experimental geometry at the seep site (Bottaro Crater, offshore Panarea, Italy) and (b) the acoustic optical lander deployed over the target seep in Bottaro Crater.

assumed volume of revolution.[7] Acoustic data were analyzed in 30 s blocks while the optics was analyzed in 15 s blocks.

III. RESULTS

In total, 368 single bubble releases were analyzed, and the results are discussed below. Natural frequencies were detected between 300 and 1000 Hz, corresponding to bubble radii between ∼0.003 and 0.012 m (Fig 3).

It is useful to examine the energy released by a bubble oscillation as the degree of variation gives us an insight into how consistent the process is. The energy emitted during a bubble's oscillation varies across nearly 3 orders of magnitude, 10^{-14}–10^{-11} J, with a mean value of 7.5×10^{-13} J. Plotting the energy released against the equilibrium bubble radius [Fig. 3(a)], we see a large degree of scatter for $R_0 < 0.006$ m, decreasing for $R_0 > 0.006$ m.

The initial amplitude of excitation of a bubble ranged mainly between 10^{-7} and 10^{-6} m with a mean value of 6.0×10^{-7} m. Plotting $R_{\varepsilon 0i}$ against the equilibrium bubble radius [Fig. 3(b)], we see a strong clustering of the data for larger bubbles ($R_0 > 0.006$ m) but, once again, a larger degree of scatter for smaller bubbles ($R_0 < 0.006$ m). Statistically, the

total correlation between R_0 and $R_{\varepsilon 0i}$, here, has a Pearson's coefficient of 0.26, a p-value of <0.001 with a trend line for R_0 and $R_{\varepsilon 0i}$ expressed in m, determined using total least squares regression (least absolute residual) of

$$R_{\varepsilon 0i} = f(R_0) = [9.608R_0 + 0.447] \times 10^{-6}, \tag{11}$$

which has a coefficient of determination of 0.99. While this relationship is highly effective for bubbles $R_0 > 0.006$ m with the 10th and 90th percentiles of the estimates being within -10% and $+15\%$ of observed values. Below $R_0 < 0.006$ m, there is a greater variability in the measurement points about the regression line with a root mean square error of 2.6×10^{-7} m compared to an average value of 6×10^{-7} m.

IV. DISCUSSION AND APPLICATION TO THE PANAREA CASE STUDY

A. Discussion of tank data results

There is a weak but statistically significant, positive correlation between $R_{\varepsilon 0i}$ and R_0 in the results here, particularly, at larger bubble sizes. This contrasts with prior work which assumes that $R_{\varepsilon 0i} = \chi_{rad} R_0$ for a constant χ_{rad}. It is important to note that the relationship developed here is an empirical one, which is not based on a physical model, and should only be applied to bubble sizes outside the range tested with care. To test the validity of this relationship for bubbles smaller than those tested here, the results are plotted alongside those of a previous study[19,32,34] [Fig. 3(c)], where observed bubbles ranged in size from ∼0.0001 to 0.001 m. Note that this is not a like for like comparison as the experiments use different generation mechanisms: sheared bubbles in a hydrodynamic current at 2 m water depth and releasing bubbles from sediment. Despite the methodological differences, the trend line derived passes through the center of the data cloud for the previous experiment and is in general good agreement down to the smallest bubble sizes, suggesting that this model is applicable across a wider range of bubble sizes than just those studied herein.

Previous assumptions about $R_{\varepsilon 0i}$ were made by Bergès et al.[19] who used the 25th and 75th percentile of the $R_{\varepsilon 0i}$ observations of Deane and Stokes[34] to invert gas flux from needles and porous stones in a test tank. Comparing our estimates of $R_{\varepsilon 0i}$ to those used by Bergès et al. when inverting gas flux in Fig. 3(b), we note that their assumption is consistent with our $R_{\varepsilon 0i}$ observation between $R_0 = $ ∼0.0001 and 0.003 m, where this is below the range of most bubble sizes observed here. This is consistent with the previous results, only suggesting that the error bounds provided were more conservative than necessary. However, as (1) bubbles were released via a different mechanism, meaning that $R_{\varepsilon 0i}$ can be expected to vary slightly; and (2) the bubble sizes ranged between 0.001 and 0.004 m radius, meaning that the majority of $R_{\varepsilon 0i}$ calculations were consistent with this study [Fig. 3(c)].

This highlights the need for researchers using acoustic flux inversion techniques in the field to compare their natural site to that used to calibrate. How similar the range of
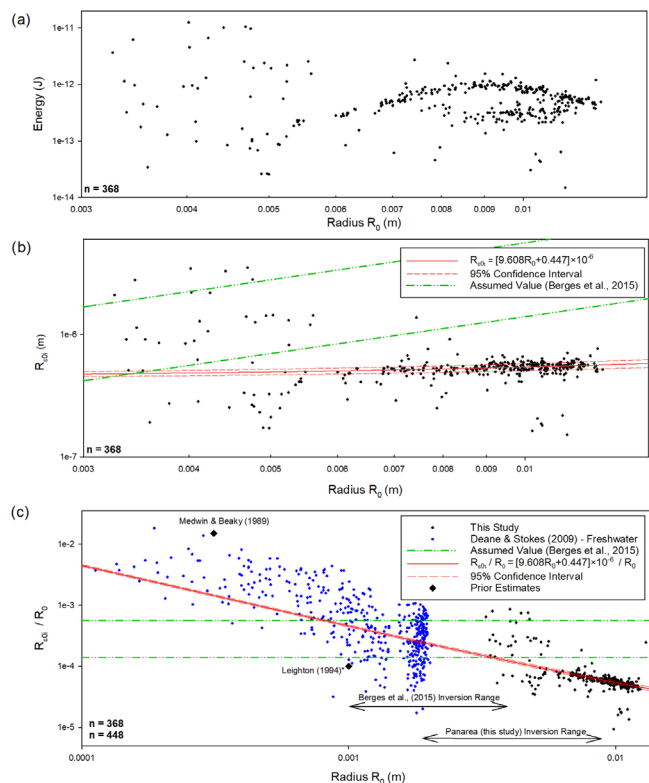
FIG. 3. (Color online) The experimental results from the analysis of single bubbles showing (a) energy released by a bubbles oscillation vs its equilibrium radius R_0 and (b) the initial amplitude of excitation $R_{\varepsilon 0i}$ vs the equilibrium radius. The lines of best fit are shown in red alongside the assumed $R_{\varepsilon 0i}$ values in Bergès et al. (Ref. 19) in green, (c) the initial amplitude of excitation of bubbles normalized by the equilibrium radius (χ_{rad}) vs the equilibrium radius from this study (black) alongside results from Deane and Stokes (Ref. 34; in blue) and other prior studies (black diamonds). Also shown is the range of bubble sizes used in Berges et al. and this study during passive acoustic flux inversion.

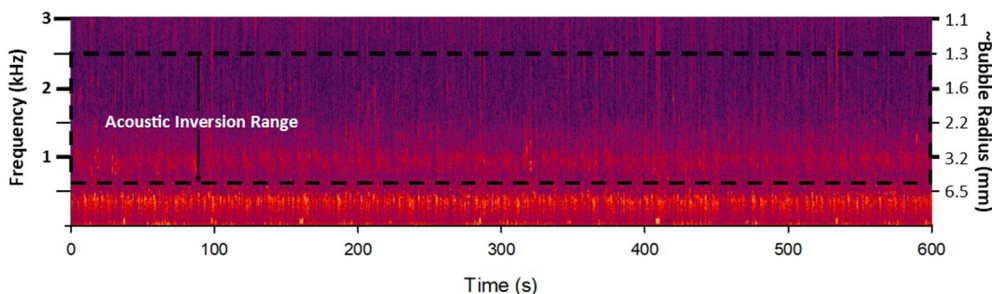FIG. 4. (Color online) The acoustic spectrogram of natural CO_2 as recorded in Panarea during a 10 min observation period with the radius of a bubble that would be responsible for a given frequency displayed on the right axis.

bubble sizes, flux rates, release mechanisms (needles, sediment type, etc.), depths, or even free field conditions are between the two will determine how accurate the $R_{\varepsilon 0i}$ estimates will be. Here, an empirical linear relationship between $R_{\varepsilon 0i}$ and R_0 has been established for these specific experimental conditions (bubbles released from course sediment in fresh water at 2.5 m depth at a slow rate of a few bubbles per second). The limits of the conditions under which this relationship can reasonably predict the bubble excitation have not been established.

While our data shows a greater variability in $R_{\varepsilon 0i}$ at smaller bubble sizes, this has little impact on the accuracy of the passive acoustic inversion technique as larger bubbles (for whom we are able to more accurately predict $R_{\varepsilon 0i}$) dominate the total volume of gas emitted (i.e., 1000 bubbles with a radius of 0.0006 m contribute the same volume of gas as one bubble with a radius of 0.006 m). Hence, in the field, it is more important for flux inversion purposes to accurately calculate $R_{\varepsilon 0i}$ for large bubbles.

B. Application to data from Panarea

To test the effectiveness of the passive acoustic inversion technique based on Eq. (11), the flux from data collected in Panarea (see Sec. II B) was compared to that recorded by other techniques. A preliminary analysis of the acoustic data revealed a strong continuous signal below ~500 Hz (Fig. 4). As optical footage suggested very few bubbles larger than 0.006 m in radius (Fig 5), $f_0 = 540$ Hz were released, we consider this low frequency noise to likely be the result of moving sediment grains and/or distant seeps.[20] Hence, the acoustic inversion is performed between 600 and 2500 Hz (corresponding to bubble radii between 0.001 and 0.005 m) to avoid interference from non-bubble related signals. The upper and lower estimates of our refined acoustic inversion were created assuming a 15% error in $R_{\varepsilon 0i}$ based on the 95% confidence interval.

The acoustic inversion technique employing Eq. (11) produces a bubbles size distribution (modal bubble radius 0.0047 m) similar to that produced used by Bergès et al. (modal bubble radius 0.0044 m)[19] with slightly more small bubbles reported by the old inversion technique (Fig. 5). Optical inversion of the Panarea data measured a single peak in the bubble size distribution at 0.0034 ± 0.0006 m.

The flux results of our refined inversion technique using Eq. (11) are presented in Fig. 6 alongside prior inversion results, assuming that χ_{Rad} is between 1.4×10^{-4} and 5.6×10^{-4}. Our refined inversion technique estimate of the gas flux is 3.2 ± 0.6 L/min, significantly greater than that predicted by the previous acoustic inversion technique $(0.8 \pm 0.7$ L/min) but consistent with the mean flux value derived via optical inversion $(3.0 \pm 0.8$ L/min). Note that the uncertainty in the method based on Eq. (11) has reduced by 78% over that employed by the previous method (reducing from 88% to 19%). However, the gas flux estimated by the refined acoustic inversion is slightly higher, 5%–8%, than that obtained by the physical measurement taken prior to deploying the lander (2.3 L/min). The failure of the prior inversion technique to match other flux estimates here is due to the larger bubble sizes seen in Panarea, since it is based on extrapolating $R_0 = 0.002$ m to larger bubbles [Fig. 3(d)].

The overestimate in the acoustic inversion estimates of flux performed using more accurate values of $R_{\varepsilon 0i}$ could be the result of, at least, two possible factors: (1) the role of seabed and sea surface reflections and (2) secondary bubbles oscillations after release.[17,24] To address the first possibility, a model of the direct acoustic path to the hydrophone along with the path reflecting off the seafloor to the hydrophone
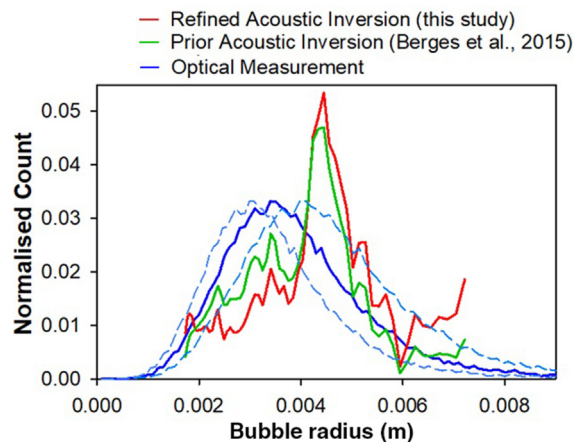

FIG. 5. (Color online) The equilibrium bubble radius distribution as estimated by each technique during a 10 min period, showing the refined acoustic inversion technique developed in this study (red), the previous acoustic inversion technique based on assuming that χ_{Rad} is constant: (green) and optical inversion (blue). The upper and lower estimates of the optical measurements are shown via blue dashed lines.

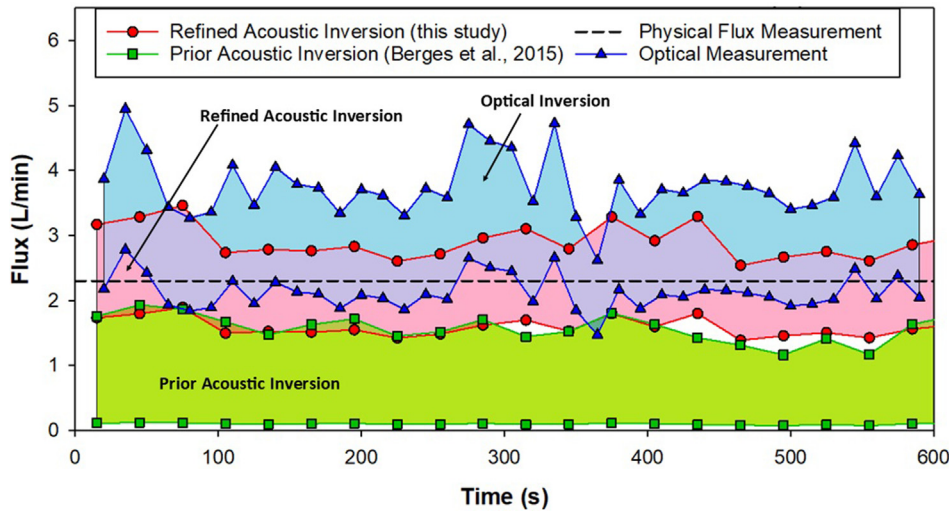804   J. Acoust. Soc. Am. **152** (2), August 2022

Roche *et al.*

FIG. 6. (Color online) The gas flux estimate via each technique across the 10 min period, the refined acoustic inversion technique developed in this study (red), the previous acoustic inversion technique based on assuming that χ_{Rad} is constant: (green) optical inversion and (blue) alongside the physical diver measurement taken prior to deployment (dashed black line).

was formed. This suggested that the energy of the reflected signal is <10% of the direct path, meaning its contribution to the overall overestimation of the flux is too small to explain the discrepancy. This would suggest that the most likely explanation for our overestimate is additional bubble oscillation occurring within the water column as bubbles merge or fragment. Wide-area video footage at Panarea shows multiple bubbles fragmenting in the water column, and this evidence is reinforced when consideration is given to the comparison of the bubble size distribution determined by optical and acoustic techniques. It may be that large bubbles are released at the seafloor where they are recorded by the hydrophone but not the optics, as they are out of thr camera's field of view. By the time the bubbles rise ~0.75 m into the view of the camera, some have fragmented into smaller bubbles, and these smaller bubbles are measured by the optics for the first time and the acoustics for a second time, resulting in the secondary acoustic peak alongside the optical peak at ~0.0035 m. In summary, further developments are needed in the acoustic flux inversion code to account for this complex bubble behavior.

As the precision of acoustic inversion techniques improve it will become increasingly more important to quantify the effect of secondary oscillations. To do so, researchers will need some gauge of how frequently bubbles from the seep are fragmenting or merging as compared to the rate of release. This almost certainly varies from seep to seep based on the number of factors, such as the bubble size distribution, where larger bubbles are more likely to fragment,[42] and the rate of release itself, with bubbles released in rapid succession being more likely to merge together.[17] One could attempt to adapt breakup frequency equations for some indication of the rate of secondary oscillation, however, these typically assume turbulent flows, unlike those seen at the seep here, and does not account for bubbles merging.[43] Assuming that secondary oscillation is solely responsible for our overestimate of flux, then the resulting scale factor would be between 0.6 and 0.9.

V. CONCLUSION

To improve quantification of gas flux from natural seeps and anthropogenic sources by passive acoustic techniques,

we have investigated the initial amplitude of the excitation of bubbles, $R_{\varepsilon 0i}$, released from coarse sediment at 2.5 m water depth, a previously unknown parameter in the inversion process.

We have empirically determined a relationship between $R_{\varepsilon 0i}$ and the equilibrium radius of a bubble, R_0 (in m), of the form $R_{\varepsilon 0i} = [9.608R_0 + 0.447] \times 10^{-6}$.

Our data show a weak positive correlation, especially at larger bubble sizes, and appears generally consistent with prior investigations of smaller (<1 mm) bubbles.

We demonstrate the potential of our refined inversion technique by inverting the flux from a natural CO_2 seep in Panarea (Italy) and comparing the results to simultaneous optical measurements. Here, we find that after filtering out low frequency, non-bubble related noise, our acoustic flux estimate is consistent with optical measurements and only 5%–8% larger than prior physical measurements. We identify the post release fragmentation of bubbles as a likely explanation of minor overestimation of flux.

The 78% improvement in the precision of the acoustic inversion technique demonstrated here will allow for the more widespread adoption of passive acoustic techniques for the long-term observations of natural seeps and the measuring, monitoring, and verification (MMV) of secure CCS sites.[6]

ACKNOWLEDGMENTS

J. Acoust. Soc. Am. **152** (2), August 2022

Roche *et al.*   805

[1]J. Blackford, Y. Artioli, J. Clark, and L. de Mora, "Monitoring of offshore geological carbon storage integrity: Implications of natural variability in the marine system and the assessment of anomaly detection criteria," Int. J. Greenhouse Gas Control **64**, 99–112 (2017).

[2]M. Razaz, D. di Iorio, B. Wang, S. Daneshgar Asl, and A. M. Thurnherr, "Variability of a natural hydrocarbon seep and its connection to the ocean surface," Sci. Rep. **10**(1), 12654 (2020).

[3]D. Oppo, L. de Siena, and D. B. Kemp, "A record of seafloor methane seepage across the last 150 million years," Sci. Rep. **10**(1), 2562 (2020).

[4]J. Blackford, H. Stahl, J. M. Bull, B. J. P. Bergès, M. Cevatoglu, A. Lichtschlag, D. Connelly, R. H. James, J. Kita, D. Long, M. Naylor, K. Shitashima, D. Smith, P. Taylor, I. Wright, M. Akhurst, B. Chen, T. M. Gernon, C. Hauton, M. Hayashi, H. Kaieda, T. G. Leighton, T. Sato, M. D. J. Sayer, M. Suzumura, K. Tait, M. E. Vardy, P. R. White, and S. Widdicombe, "Detection and impacts of leakage from sub-seafloor deep geological carbon dioxide storage," Nat. Clim. Change **4**(11), 1011–1016 (2014).

[5]M. Dean, J. Blackford, D. Connelly, and R. Hines, "Insights and guidance for offshore CO_2 storage monitoring based on the QICS, ETI MMV, and STEMM-CCS projects," Int. J. Greenhouse Gas Control **100**, 103120 (2020).

[6]M. Dean and O. Tucker, "A risk-based framework for measurement, monitoring and verification (MMV) of the Goldeneye storage complex for the Peterhead CCS project, UK," Int. J. Greenhouse Gas Control **61**, 1–15 (2017).

[7]J. Li, P. R. White, B. Roche, J. M. Bull, T. G. Leighton, J. W. Davis, and J. W. Fone, "Acoustic and optical determination of bubble size distributions—Quantification of seabed gas emissions," Int. J. Greenhouse Gas Control **108**, 103313 (2021).

[8]B. Wang and S. A. Socolofsky, "A deep-sea, high-speed, stereoscopic imaging system for *in situ* measurement of natural seep bubble and droplet characteristics," Deep Sea Res., Part I **104**, 134–148 (2015).

[9]A. Jordt, C. Zelenka, J. S. von Deimling, R. Koch, and K. Köser, "The Bubble Box: Towards an automated visual sensor for 3D analysis and characterization of marine gas release sites," Sensors **15**(12), 30716–30735 (2015).

[10]J. Li, B. Roche, J. M. Bull, P. R. White, T. G. Leighton, G. Provenzano, M. Dewar, and T. J. Henstock, "Broadband acoustic inversion for gas flux auantification—Application to a methane plume at Scanner Pockmark, Central North Sea," J. Geophys. Res.: Oceans **125**(9), e2020JC016360, https://doi.org/10.1029/2020JC016360 (2020).

[11]J. Schneider von Deimling, P. Linke, M. Schmidt, and G. Rehder, "Ongoing methane discharge at well site 22/4b (North Sea) and discovery of a spiral vortex bubble plume motion," Mar. Pet. Geol. **68**, 718–730 (2015).

[12]J. Greinert, "Monitoring temporal variability of bubble release at seeps: The hydroacoustic swath system GasQuant," J. Geophys. Res. **113**(C7), C07048, https://doi.org/10.1029/2007JC004704 (2008).

[13]J. Greinert, Y. Artemov, V. Egorov, M. Debatist, and D. McGinnis, "1300-m-high rising bubbles from mud volcanoes at 2080 m in the Black Sea: Hydroacoustic characteristics and temporal variability," Earth Planet. Sci. Lett. **244**(1–2), 1–15 (2006).

[14]K. Baik, T. G. Leighton, and J. Jiang, "Investigation of a method for real time quantification of gas bubbles in pipelines," J. Acoust. Soc. Am. **136**(2), 502–513 (2014).

[15]T. G. Leighton, K. Baik, and J. Jiang, "The use of acoustic inversion to estimate the bubble size distribution in pipelines," Proc. R. Soc. A **468**(2145), 2461–2484 (2012).

[16]L. Chen, V. Trinh, W. Yang, and K. Mohanangam, "Prediction of bubble generation based on acoustic emission," Acoust. Aust. **44**(2), 325–331 (2016).

[17]T. G. Leighton, K. J. Fagan, and J. E. Field, "Acoustic and photographic studies of injected bubbles," Eur. J. Phys. **12**(2), 77–85 (1991).

[18]J. Li, P. R. White, J. M. Bull, T. G. Leighton, B. Roche, and J. W. Davis, "Passive acoustic localisation of undersea gas seeps using beamforming," Int. J. Greenhouse Gas Control **108**, 103316 (2021).

[19]B. J. P. Bergès, T. G. Leighton, and P. R. White, "Passive acoustic quantification of gas fluxes during controlled gas release experiments," Int. J. Greenhouse Gas Control **38**, 64–79 (2015).

[20]A. Vazquez, R. Manasseh, and R. Chicharro, "Can acoustic emissions be used to size bubbles seeping from a sediment bed?," Chem. Eng. Sci. **131**, 187–196 (2015).

[21]T. G. Leighton and P. R. White, "Quantification of undersea gas leaks from carbon capture and storage facilities, from pipelines and from methane seeps, by their acoustic emissions," Proc. R. Soc. A **468**(2138), 485–510 (2012).

[22]M. S. Longuet-Higgins, B. R. Kerman, and K. Lunde, "The release of air bubbles from an underwater nozzle," J. Fluid Mech. **230**, 365–390 (1991).

[23]H. Czerski and G. B. Deane, "Contributions to the acoustic excitation of bubbles released from a nozzle," J. Acoust. Soc. Am. **128**(5), 2625–2634 (2010).

[24]T. G. Leighton and A. J. Walton, "An experimental study of the sound emitted from gas bubbles in a liquid," Eur. J. Phys. **8**(2), 98–104 (1987).

[25]H. C. Pumphrey and J. E. Ffowcs Williams, "Bubbles as sources of ambient noise," IEEE J. Ocean. Eng. **15**(4), 268–274 (1990).

[26]M. Minnaert, "XVI. On musical air-bubbles and the sounds of running water," London, Edinburgh, Dublin Philosoph. Mag. J. Sci. **16**(104), 235–248 (1933).

[27]T. G. Leighton, "The freely-oscillating bubble," in *The Acoustic Bubble* (Academic, New York, 1994), pp. 129–286.

[28]T. G. Leighton, P. R. White, and M. F. Schneider, "The detection and dimension of bubble entrainment and comminution," J. Acoust. Soc. Am. **103**(4), 1825–1835 (1998).

[29]M. R. Loewen and W. K. Melville, "An experimental investigation of the collective oscillations of bubble plumes entrained by breaking waves," J. Acoust. Soc. Am. **95**(3), 1329–1343 (1994).

[30]J. Li, P. R. White, J. M. Bull, T. G. Leighton, B. Roche, and J. W. Davis, "Passive acoustic monitoring of a natural CO_2 seep site—Implications for carbon capture and storage," Int. J. Greenhouse Gas Control **93**, 102899 (2020).

[31]T. G. Leighton, "The Rayleigh–Plesset equation in terms of volume with explicit shear losses," Ultrasonics **48**(2), 85–90 (2008).

[32]T. G. Leighton, *The Acoustic Bubble* (Academic, New York, 1994).

[33]H. Medwin and M. M. Beaky, "Bubble sources of the Knudsen sea noise spectra," J. Acoust. Soc. Am. **86**(3), 1124–1130 (1989).

[34]G. B. Deane and M. D. Stokes, "The acoustic excitation of air bubbles fragmenting in sheared flow," J. Acoust. Soc. Am. **124**(6), 3450–3463 (2008).

[35]T. Monecke, S. Peterson, M. D. Hannington, M. Anzidei, A. Esposito, G. Giordano, D. Garbe-Schönberg, N. Augustin, B. Melchert, and M. Hocking, "Explosion craters associated with shallow submarine gas venting off Panarea island, Italy," Bull. Volcanol. **74**(9), 1937–1944 (2012).

[36]S. Caliro, A. Caracausi, G. Chiodini, M. Ditta, F. Italiano, M. Longo, C. Minopoli, P. M. Nuccio, A. Paonita, and A. Rizzo, "Evidence of a recent input of magmatic gases into the quiescent volcanic edifice of Panarea, Aeolian Islands, Italy," Geophys. Res. Lett. **31**(7), L07619, https://doi.org/10.1029/2003GL019359 (2004).

[37]S. Inguaggiato, I. S. Diliberto, C. Federico, A. Paonita, and F. Vita, "Review of the evolution of geochemical monitoring, networks and methodologies applied to the volcanoes of the Aeolian Arc (Italy)," Earth-Sci. Rev. **176**, 241–276 (2018).

[38]E. Bagnato, E. Oliveri, A. Acquavita, S. Covelli, E. Petranich, M. Barra, F. Italiano, F. Parello, and M. Sprovieri, "Hydrochemical mercury distribution and air-sea exchange over the submarine hydrothermal vents offshore Panarea Island (Aeolian arc, Tyrrhenian Sea)," Mar. Chem. **194**, 63–78 (2017).

[39]M. Molari, K. Guilini, L. Lins, A. Ramette, and A. Vanreusel, "CO_2 leakage can cause loss of benthic biodiversity in submarine sands," Mar. Environ. Res. **144**, 213–229 (2019).

[40]S. Quale and V. Rohling, "The European Carbon dioxide Capture and Storage Laboratory Infrastructure (ECCSEL)," Green Energy Environ. **1**(3), 180–194 (2016).

[41]G. Caramanna, N. Voltattorni, and M. M. Maroto-Valer, "Is Panarea Island (Italy) a valid and cost-effective natural laboratory for the development of detection and monitoring techniques for submarine CO_2 seepage?," Greenhouse Gases: Sci. Technol. **1**(3), 200–210 (2011).

[42]K. Tsuchiya, K. Ohsaki, and K. Taguchi, "Large and small bubble interaction patterns in a bubble column," Int. J. Multiphase Flow **22**(1), 121–132 (1996).

[43]C. Martínez-Bazán, J. L. Montañés, and J. C. Lasheras, "On the breakup of an air bubble injected into a fully developed turbulent flow. Part 1. Breakup frequency," J. Fluid Mech. **401**, 157–182 (1999).

806   J. Acoust. Soc. Am. **152** (2), August 2022

Roche *et al.*

31 August 2024 10:12:24